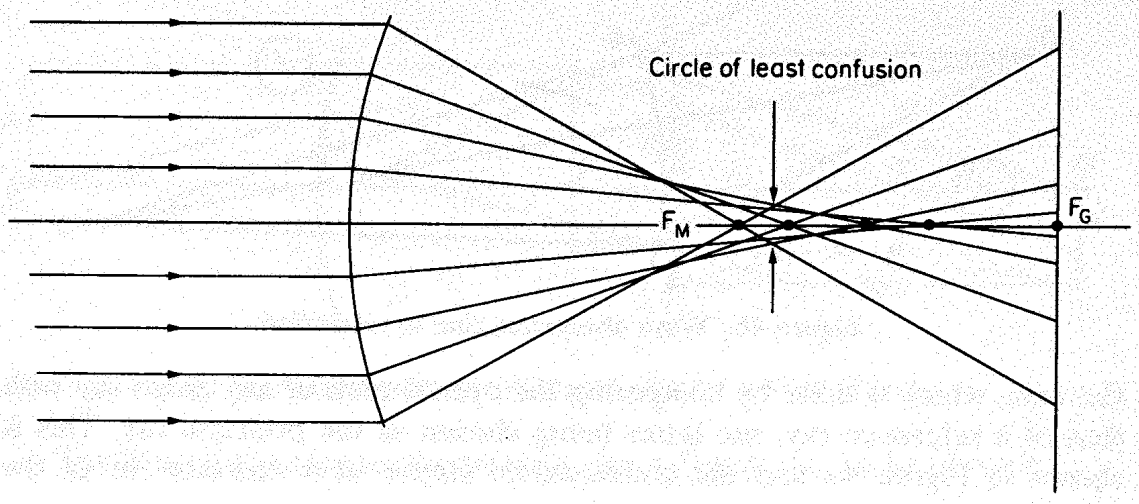

Figure 5a. Spherical aberration

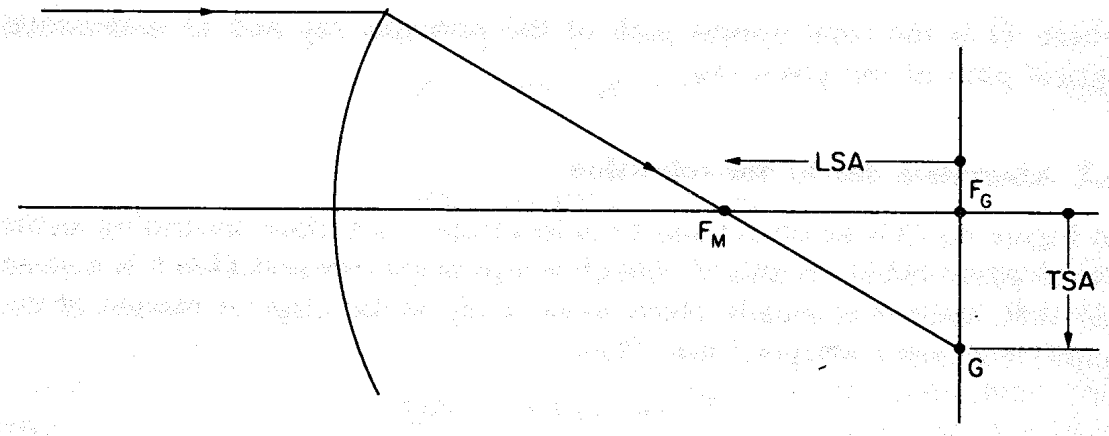

Figure 5b. Longitudinal and transverse spherical aberration

obtained from the paraxial ray tracing equations. The distance along the axis between the marginal focus F_M and the Gaussian focus F_G is the longitudinal spherical aberration, LSA. The distance between F_G and the marginal ray intercept G on the Gaussian image plane is the transverse spherical aberration, TSA. Similar results are obtained for off-axis objects, as shown in Figure 5c. Suppose Figure 4b is redrawn explicitly for an axial object, as shown in Figure 5d, such that $\bar{A}A$ is a surface, centre C, radius r, separating media of refractive indices n and n', α is the angle subtended at the centre by $\bar{A}A$, and i is the angle of incidence of a marginal ray OA, from an axial object O. H is the foot of the perpendicular from A to the axis $O\bar{A}C$,

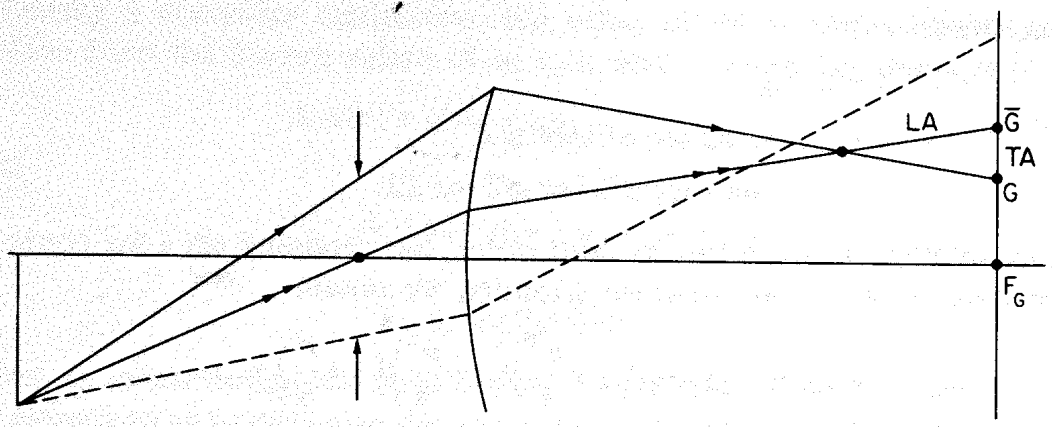

Figure 5c. Longitudinal and transverse aberration for an off-axis object

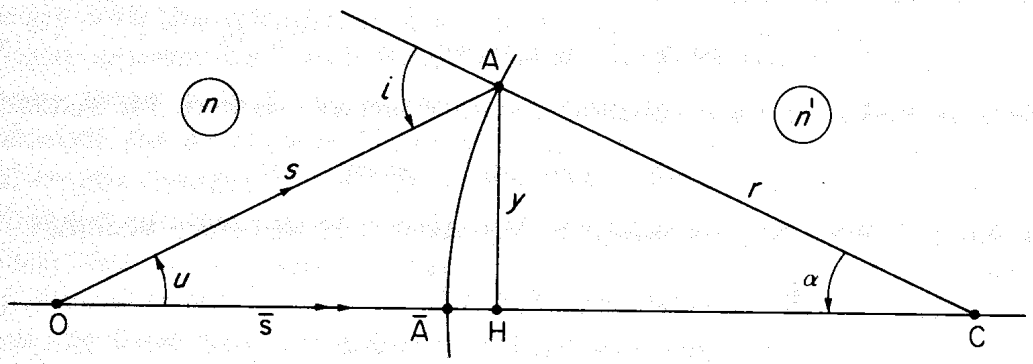

Figure 5d. Calculation of wavefront aberration

$HA = y$, $\bar{A}O = \bar{s}$ and $AO = s$. Then, from Figure 5d,

$$AH = r(1-\cos\alpha),$$

and

$$OH = \bar{s} + r(1-\cos\alpha) = s\cos u.$$

Therefore

$$\bar{A}O - AO = \bar{s} - s = s(\cos u - 1) + r(\cos\alpha - 1)$$

Now

$$y = s\sin u = r\sin\alpha,$$

hence

$$\begin{aligned}\bar{s} - s &= y[(\cos u - 1)/\sin u + (\cos\alpha - 1)/\sin\alpha] \\ &= -y(\tan u/2 + \tan\alpha/2) \\ &= -y[\sin(u/2)\cos(\alpha/2) + \sin(\alpha/2)\cos(u/2)]\sec(\alpha/2)\sec(u/2) \\ &= -y\sin\left(\frac{u+\alpha}{2}\right)\sec(\alpha/2)\sec(u/2).\end{aligned}$$

Thus, since

$$i = u + \alpha,$$
$$\bar{s} - s = -y \sin i/2 \sec \alpha/2 \sec u/2$$
$$= -\tfrac{1}{2} y \sin i \sec \alpha/2 \sec u/2 \sec i/2.$$

On expanding the sec terms to third order, but retaining sin i for convenience since $n \sin i$ is an invariant quantity, we obtain

$$\bar{s} - s = -\tfrac{1}{2} y \sin i \left(1 + \frac{\alpha^2}{8}\right)\left(1 + \frac{u^2}{8}\right)\left(1 + \frac{i^2}{8}\right) + \ldots$$
$$= -\tfrac{1}{2} y \sin i - \tfrac{1}{16} y \sin i(\alpha^2 + u^2 + i^2) + \ldots.$$

We then find, from equation (20), that

$$W = -\tfrac{1}{2}\Delta(yn \sin i) - \tfrac{1}{16}\Delta(yn \sin i(\alpha^2 + u^2 + i^2) \ldots). \tag{21}$$

Now y, α, and $n \sin i$ are constant across a surface, so that, for instance

$$\Delta(yn \sin i) = yn' \sin i' - yn \sin i = 0$$

and similarly for terms including α. Equation (21) therefore becomes

$$W = -\tfrac{1}{16} y(n \sin i)\Delta(u^2 + i^2)$$
$$= -\tfrac{1}{16} y(n \sin i)\Delta[(i - u)^2 + 2ui]$$
$$= -\tfrac{1}{16} y(n \sin i)\Delta(\alpha^2 + 2ui)$$
$$= -\tfrac{1}{8} y(n \sin i)\Delta(ui)$$
$$= -\tfrac{1}{8} y(n \sin i)\Delta\left[\frac{u}{n}(n \sin i)\frac{i}{\sin i}\right]$$
$$= -\tfrac{1}{8} y(n \sin i)^2 \Delta\left(\frac{u}{n}\right)(1 + \tfrac{1}{6}\sin^2 i + \ldots),$$

where we have used

$$i = \sin i + \tfrac{1}{6}(\sin^3 i) + \ldots.$$

Finally, expanding to third order in i gives, for the first term $S1$ of W,

$$S1 = -\tfrac{1}{8} y A^2 \Delta(u/n), \tag{22}$$

in which $A = ni$, is the paraxial value of the Snell refraction invariant. (Note, it is the convention to denote by S_I—in which S stands for Seidel, one of the earliest investigators of lens aberrations[3]—the value $-yA^2\Delta(u/n)$, so that $S1 = \frac{1}{8} S_I$.) As a consequence of refraction each surface therefore contributes to the wavefront spherical aberration an amount equal to $S1$ and it can be shown that the total aberration to third order for a system of surfaces is equal to the sum of the contributions at each surface as the transfer process produces no new aberration.[4]

During a computer calculation, the value of $S1$ is determined at each surface from the known values of n, c, u, and y, using the identities

$$\Delta(u/n) = u'/n' - u/n,$$

and

$$A = ni = n(u+\alpha) = nu + nyc.$$

6. BENDING

After an initial design has been set up, and its aberration calculated, it can be altered so as to minimize the aberration. The simplest way to do this is to leave the glass types and separations unchanged, but to alter the curvatures of the surfaces in a systematic way, because the aberration varies quite strongly with this parameter. The easiest way to do this would be to add a constant amount Δc to each curvature, so that positively curved surfaces become more curved and negatively curved surfaces less so, and then to recalculate the aberration. However, it is found that if this is done then the focal length changes and a way to avoid this, as first shown by Hopkins,[5] is to alter the curvature in such a way that the angle α is changed by a constant amount $\Delta\alpha$, or in other words to make Δc at each surface inversely proportional to the height y so that $\Delta\alpha = y\Delta c$ is constant. The fact that this leaves the focal length unchanged will now be demonstrated.

As shown earlier, equation (6), the equation for refraction at each surface can be written as

$$n'_s u'_s - n_s u_s = -(n'_s - n_s)\alpha_s.$$

Writing this out in full for each surface we have

$$\begin{aligned} n'_1 u'_1 - n_1 u_1 &= (n_1 - n'_1)\alpha_1, \\ n'_2 u'_2 - n_2 u_2 &= (n_2 - n'_2)\alpha_2, \\ n'_J u'_J - n_J u_J &= (n_J - n'_J)\alpha_J, \end{aligned}$$

so that on adding, and using the fact that

$$n_2 = n'_1, \qquad u_2 = u'_1, \ldots$$

we find that

$$n'_J u'_J - n_1 u_1 = n_1\alpha_1 - n'_J\alpha_J + \sum n_J(\alpha_J - \alpha_{J-1}).$$

It is usual in an optical system for the initial and final refractive indices to be the same, that is (for air),

$$n'_J = n_1 = 1.0$$

so that

$$u'_J - u_1 = (\alpha_1 - \alpha_J) + \sum n_J(\alpha_J - \alpha_{J-1}) \tag{23}$$

If, in equation (23), each value of α is altered by the same amount $\Delta\alpha$ it is seen that the right-hand side remains unchanged, hence for a given u_1 the final angle u'_J is unaltered and it follows, from equation (11), that the focal length of the system stays at its initial value.

6.1 Effect of bending

The effect of bending is to make $S1$ vary as a parabolic function of $\Delta\alpha$ (see Figure 8c) that may or may not pass through the $\Delta\alpha$ axis. In the former case the choice of lens shape will depend on the presence of other aberrations, especially the asymmetric aberration known as coma which is often a minimum near the turning point (not zero) value of $S1$. In the latter case the numerically minimum value of $S1$ may be brought closer to zero by altering the refractive indices or separations, but this cannot always be done in a systematic manner—as can bending—and is outside the scope of this chapter.

7. FINITE RAY TRACING

So far we have considered only the paraxial approximation that has allowed us to determine the focal length, the Gaussian image plane, and a measure of the wavefront spherical aberration and its variation with lens shape.

When a design has approached a sufficient minimum in aberration—which may require changes in refractive indices and element separations as well as changes in curvatures—then it is time to trace some actual rays through the system and determine how these are spread out over the image plane.

To trace the actual paths of rays means that we must determine the true heights Y and angles U at which a ray strikes a surface rather than their paraxial approximations y and u.

The procedure for doing this which is called finite ray tracing makes use of Snell's law and coordinate geometry.

7.1 Finite ray tracing in two dimensions

Consider an optical system that has an axis of symmetry OZ and with the OYZ plane containing the off-axis object point. The plane OYZ is called the meridian plane and it is a consequence of Snell's law, and the axial symmetry, that a ray which leaves the object in this plane will remain in it. The process of tracing such a ray thus involves only two-dimensional geometry which simplifies the analysis to a certain extent, as we shall now see. Figure 6a shows a ray $\tilde{P}P$ leaving a surface at $\tilde{P}$, with known coordinates $(\tilde{Y}, \tilde{Z})$, and proceeding at a known angle U with the axis to the next surface, centre C, radius r, distance t along the axis, which it intersects at P whose coordinates are (Y, Z) with respect to axes with origin at O.

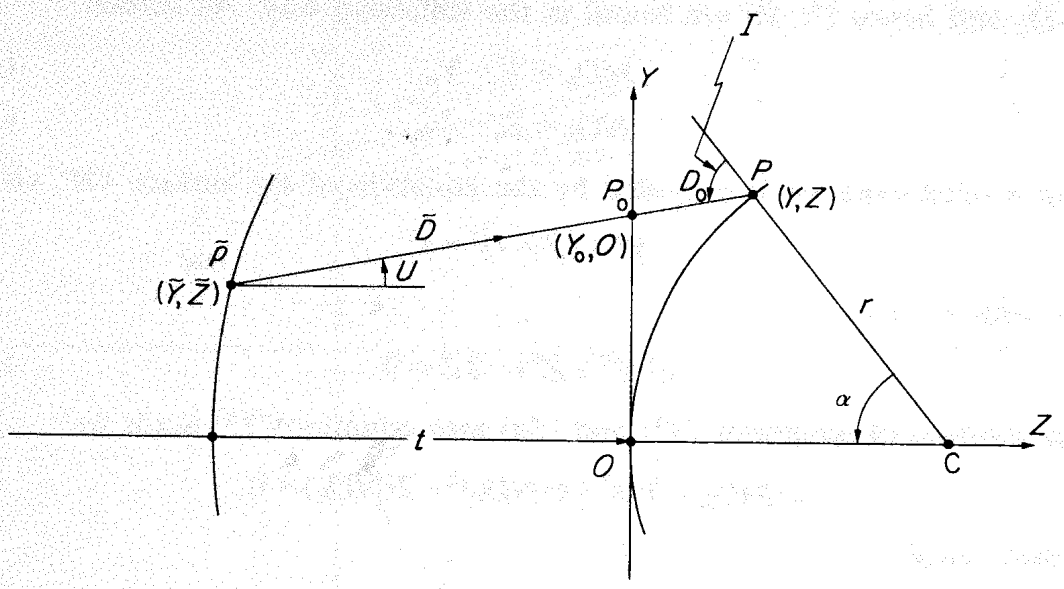

Figure 6a. Parameters for tracing a finite ray

Suppose the ray intersects the tangent plane, (at O), at point P_0 whose coordinates are $(Y_0, 0)$ and adopt the definitions

$$\tilde{P}P = D, \tag{24}$$

$$\tilde{P}P_0 = \tilde{D}, \tag{25}$$

$$P_0P = D_0. \tag{26}$$

The quantities to be determined are the coordinates (Y, Z) and the angle I that the ray $\tilde{P}P$ makes with the normal PC. If the direction cosines of the ray are

$$M = \sin U, \tag{27}$$

$$N = \cos U, \tag{28}$$

then from the figure it is seen that

$$\tilde{P}P_0 \sin U = \tilde{D}M = Y_0 - \tilde{Y}, \tag{29}$$

$$\tilde{P}P_0 \cos U = \tilde{D}N = t - \tilde{Z}. \tag{30}$$

Hence the equations

$$\tilde{D} = (t - \tilde{Z})/N, \tag{31}$$

$$Y_0 = \tilde{Y} + (t - \tilde{Z})M/N, \tag{32}$$

determine $\tilde{D}$ and Y_0 in terms of the known ray parameters. $\tilde{Z}$ is measured with respect to the origin of the first curved surface.

D_0 and hence (Y, Z) are found in the following way. As before

$$MD_0 = Y - Y_0, \tag{33}$$

$$ND_0 = Z, \tag{34}$$

and a third equation is provided by the equation of the surface OP, viz.:

$$Y^2 + (Z - r)^2 = r^2,$$

or, with $c = 1/r$,

$$c(Y^2 + Z^2) - 2Z = 0. \tag{35}$$

Substitution of equations (33) and (34) into equation (35) leads to

$$c(MD_0 + Y_0)^2 + c(ND_0)^2 - 2(ND_0) = 0,$$

which, since

$$M^2 + N^2 = 1$$

is also

$$cD_0^2 - 2(N - cMY_0)D_0 + cY_0^2 = 0.$$

Now, in accordance with standard practice,[6] we use

$$F = cY_0^2, \tag{36}$$

$$G = N - cMY_0, \tag{37}$$

which are known quantities, so that D_0 is simply a root of the quadratic equation

$$cD_0^2 - 2GD_0 + F = 0, \tag{38}$$

i.e.

$$D_0 = (G - \sqrt{G^2 - cF})/c, \tag{39}$$

where the negative sign is taken since D_0 has to be the lesser of the two possible values—as shown in Figure 6b. Equation (39), because the limit $c \to 0$ can cause numerical trouble, has a better computational form after rationalization with the numerator. Thus

$$D_0 = \frac{G - \sqrt{G^2 - cF}}{c} \frac{G + \sqrt{G^2 - cF}}{G + \sqrt{G^2 - cF}},$$

or

$$D_0 = F/(G + \sqrt{G^2 - cF}). \tag{40}$$

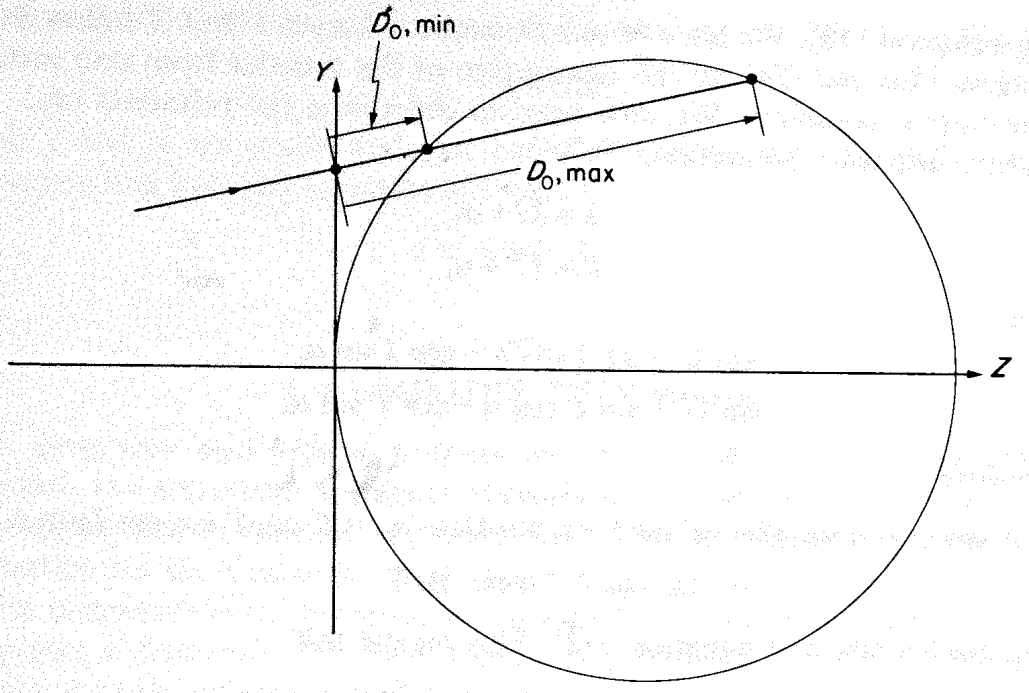

Figure 6b. Maximum and minimum values of D_0

Also, from Figure 6a,

$$I = U + \alpha,$$

therefore

$$\cos I = \cos U \cos \alpha - \sin U \sin \alpha,$$

or

$$\cos I = N \cos \alpha - M \sin \alpha,$$

whilst, from Figure 6a,

$$\cos \alpha = (r - Z)/r = 1 - cZ, \tag{41}$$

$$\sin \alpha = Y/r = cY, \tag{42}$$

hence

$$\begin{aligned} \cos I &= N - NcZ - McY \\ &= N - cN(ND_0) - cM(Y_0 + MD_0), \end{aligned}$$

using equations (33) and (34). Therefore

$$\begin{aligned} \cos I &= (N - cMY_0) - cD_0 \\ &= G - cD_0 \\ &= \sqrt{G^2 - cF}. \end{aligned} \tag{43}$$

using equation (39). We have found D_0 and cos I, and Y and Z follow from equations (33) and (34), so the description of the transfer from one surface to the next is complete. We now need to determine the refracted ray.

Before and after refraction,

$$I = U + \alpha,$$
$$I' = U' + \alpha,$$

hence

$$\sin U = \sin I \cos \alpha - \cos I \sin \alpha,$$
$$\sin U' = \sin I' \cos \alpha - \cos I' \sin \alpha.$$

Therefore

$$n' \sin U' - n \sin U = (n' \sin I' - n \sin I)\cos \alpha - (n' \cos I' - n \cos I)\sin \alpha$$
$$= -(n' \cos I' - n \cos I)cY,$$

using Snell's law and equation (42). This means that

$$n' \sin U' = n \sin U - YK, \tag{44}$$

where the power K is given by

$$K = (n' \cos I' - n \cos I)c \tag{45}$$

and $n' \cos I'$ is determined from Snell's law and the known value of cos I (equation (32)). Similarly, by considering

$$\cos U = \cos I \cos \alpha - \sin I \sin \alpha$$

one can show that

$$n' \cos U' = n \cos U - ZK + (n' \cos I' - n \cos I) \tag{46}$$

In terms of M and N equations (44) and (46) may be written as

$$n'M' = nM - YK \tag{47}$$
$$n'N' = nN - ZK + (n' \cos I' - N \cos I) \tag{48}$$

or alternatively, in two dimensions, N' may be determined from M' by using the fact that

$$M'^2 + N'^2 = 1$$

which can be used as a check on the values of M' and N'.

The derivation of the equations required for tracing a finite ray through an optical system is now complete. However, it is interesting to note that equations (33) and (29) may be combined as

$$Y = Y_0 + MD_0 = \tilde{Y} + M\tilde{D} + MD_0 = \tilde{Y} + MD$$
$$= \tilde{Y} + D \sin U$$

which reduces to the paraxial equation (8), viz.:

$$y_+ = y + d'u'$$

when y and u are small, and that equation (44) reduces, similarly, to the corresponding paraxial equation (6) viz.:

$$n'u' = nu - Ky.$$

8. COMPUTER PROGRAMS

Two programs and typical outputs are given below, one S1BEND to calculate the wavefront spherical aberration $S1$ and its variation with the bending parameter $\Delta\alpha$, and the other RAYTRC to calculate the transverse aberration on the Gaussian image plane.

The comments in the program are designed to be self-explanatory; in both programs a distinction between objects at a finite distance and objects at infinity is made by means of the logical variable FINITE. In S1BEND it is assumed that the position of a finite object is specified by the incident ray angle $U(1)$ and its height $Y(1)$ on the first surface as these are required in both cases—finite, or infinite; in RAYTRC, however, the image height must be calculated and also the initial incidence angle varies, so it is convenient to specify a finite object by its size and distance, cf. equation (10). The data required for the programs are listed in the comments. Some specific data for a typical optical system are considered in section 8.1. Besides looking at the effects of bending the S1BEND program may also be used to investigate the variation of $S1$ with angle $U(1)$ and incident height $Y(1)$ by setting the bending parameters to zero and running the program for the required incident ray parameters.

8.1 Example of data

A suitable optical system on which to try the programs is provided by the TESSAR type photographic lens, such as the one specified by O'Neill,[7] of which a diagram is shown in Figure 7 and the data are given in Table 1.

The focal length of the lens is given as (approximately) 50 mm, but further details are not given, so we shall assume therefore that it is designed to cover a 35 mm film and that it operates at a maximum relative aperture, or stop number, of f/2.8, (i.e. focal length/aperture = 2.8). Using these figures we see that the maximum semi-angle of the rays entering the lens is approximately $\tan^{-1}(17.5/50)$, i.e. 20°, whilst the aperture is given by 50/2.8 or approximately 18 mm, the semi-aperture is therefore 9 mm. The initial

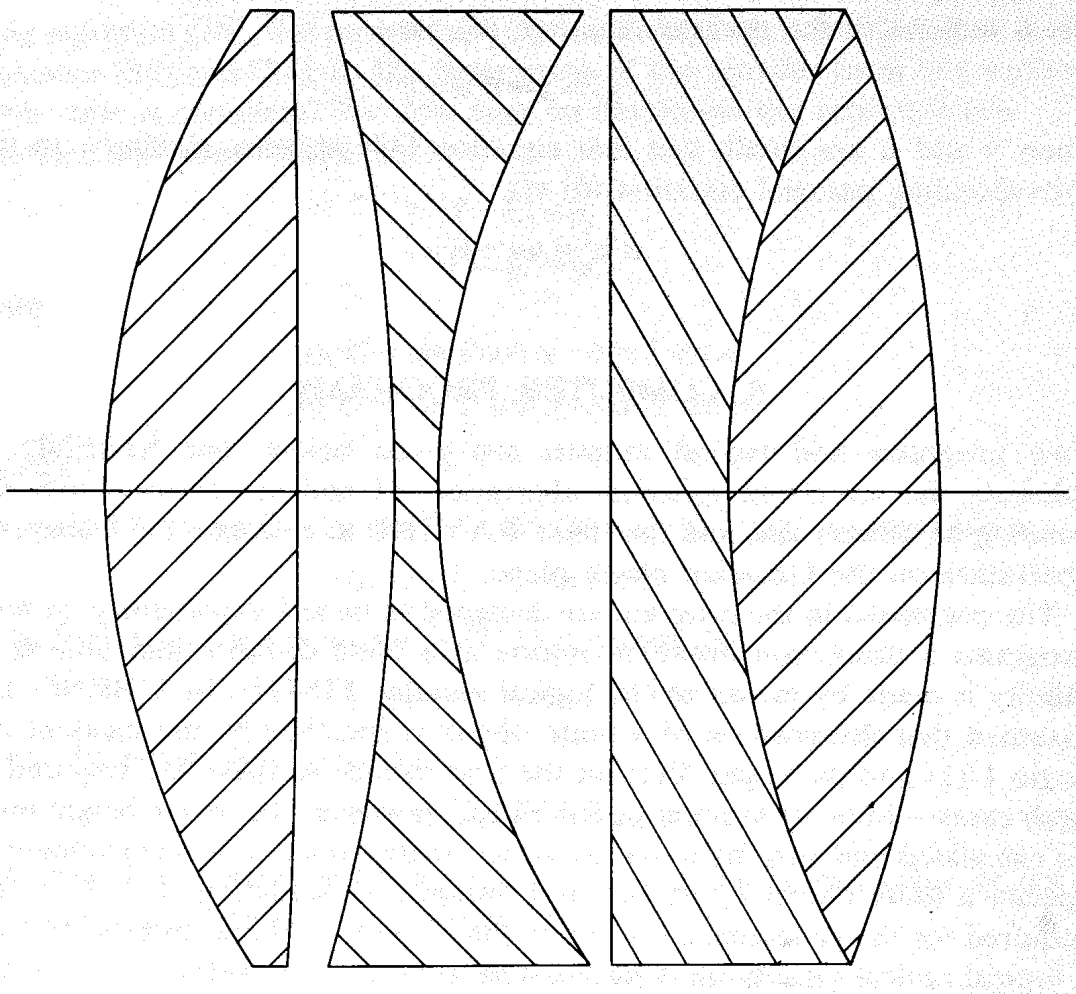

Figure 7. Diagram of the TESSAR lens

Table 1. Data for the TESSAR lens

n	c (cm^{-1})	d (cm)
1.0		
	0.61425	
1.6116		0.357
	−0.036271	
1.0		0.189
	−0.28927	
1.6053		0.081
	0.63221	
1.0		0.325
	0	
1.5123		0.217
	0.52083	
1.6116		0.396
	−0.41667	
1.0		

data for an infinite object are thus:

Logical parameter	FINITE = FALSE
Incidence height	$Y(1) = 0.9$ cm
Field angle	$U(1) = -20°$

8.2 Results from S1BEND

The aberration program S1BEND, using the initial data given in section 8.1 and zero bending (i.e. DALPH0 = 0.0, NALPH0 = 0) gives the following results

Focal length	$f' = 5.08$ cm
Spherical aberration	$S1 = -3.76 \times 10^{-3}$ cm

The focal length agrees with the quoted value of ≈5.0 cm, but we shall now have to consider the significance of the $S1$ value.

The first point to remember is that $S1$ is the difference in optical path between the marginal ray (at 20° and 0.9 cm) and the principal ray and that in an ideal optical system this should be zero. Now, superficially, $S1$ is quite small and indeed it is only about 0.075% of the focal length. (Note that the negative value means that the wave at the margin is behind the ideal spherical wave through the centre of the exit pupil.) The closeness to perfection, however, is not measured absolutely nor by comparison with the focal length but rather in terms of the wavelength of light.

Lord Rayleigh[8] was one of the first to discuss the influence of aberrations on optical image formation, and he showed that if a system is defocused then the image is expected to show no appreciable deterioration if the optical paths of the rays reaching the image region differ by less than one-quarter of a wavelength. This result is now called the Rayleigh limit and is frequently used quite generally, although it is only strictly true for a defocusing error. Subsequent work has shown that the limit can be raised and that a wavelength error of 0.95λ is tolerable for spherical aberration if some defocusing is introduced, because a better image can be found away from the Gaussian image, as shown in Figure 5a where the so-called circle of least confusion shows a sharper concentration of rays than the Gaussian image. Furthermore, if higher order spherical aberration terms are considered, that were neglected in section 5.2, then the limit can be raised to approximately 6λ.[9]

The magnitude of $S1$, i.e. 3.76×10^{-3} cm can now be looked at again in the light of these comments. For a wavelength of 590 mm, $S1$ amounts to 64λ which is on extremely large value, compared with the required value of about one wavelength. It should be said in mitigation, however, that this

Table 2. Variation of $S1$ with field angle and aperture

	$U(1)$		
$Y(1)$	$-20°$	$-10°$	$0°$
0.9	−37.6	−11.6	9.49
0.75	−20.8	−8.31	4.57
0.625	−9.65	−5.57	2.21
0.5	−1.11	−3.17	0.90
0.375	+4.78	−1.30	0.28
0.25	+8.10	−0.07	0.056
0.125	+9.04	+0.51	0.003
0	+7.84	+0.49	0
−0.125	+4.84	+0.03	0.003
−0.25	+0.48	−0.64	0.056
−0.375	−4.75	−1.20	0.28
−0.5	−10.2	−1.25	0.90
−0.625	−15.3	−0.30	2.21
−0.75	−19.2	+2.22	4.57
−0.9	−21.1	+8.26	9.49
		$\times 10^{-4}$ cm	

value of $S1$ corresponds with the extreme edge of the field and the largest aperture. A more realistic appreciation of the extent of the aberration is obtained by repeating the calculation for other values of $U(1)$ and $Y(1)$.

Table 2 contains the results obtained with S1BEND by setting the bending parameter NALPHA equal to zero and using incident heights that scan the aperture, and incident angles of $-20°$, $-10°$, and $0°$. The results are shown graphically in Figure 8a from which it can be seen that the aberration falls rapidly with incidence height and approaches a sufficiently small value for apertures less than 0.625 ($f/4$), especially for angular fields between $0°$ and $10°$. These curves show, in effect, the shape of the wavefront as a function of aperture and it is interesting to note, for example, that the spherical aberration for $(-20°, 0.75)$ is exactly $16\times$ that for $(-10°, 0.375)$. This follows from the fact that at each surface $S1$ is proportional to y, A^2, and u; in fact, for a given axial intersection point, we have: (1) $u \propto y$ and (2) $A = ni = n(u + yc) \propto y$ so that, in all, we find for each surface

$$S1 \propto y^4.$$

The proportionality does not, however, hold for the first surface as u and y can be chosen independently there, and to show the fourth-power dependence we need to halve both the initial angle of incidence and the incidence height. The curve for $U(1) = 0°$, however, follows exactly a fourth-power curve.

Typical results that show the effect of bending the lens are given, in part,

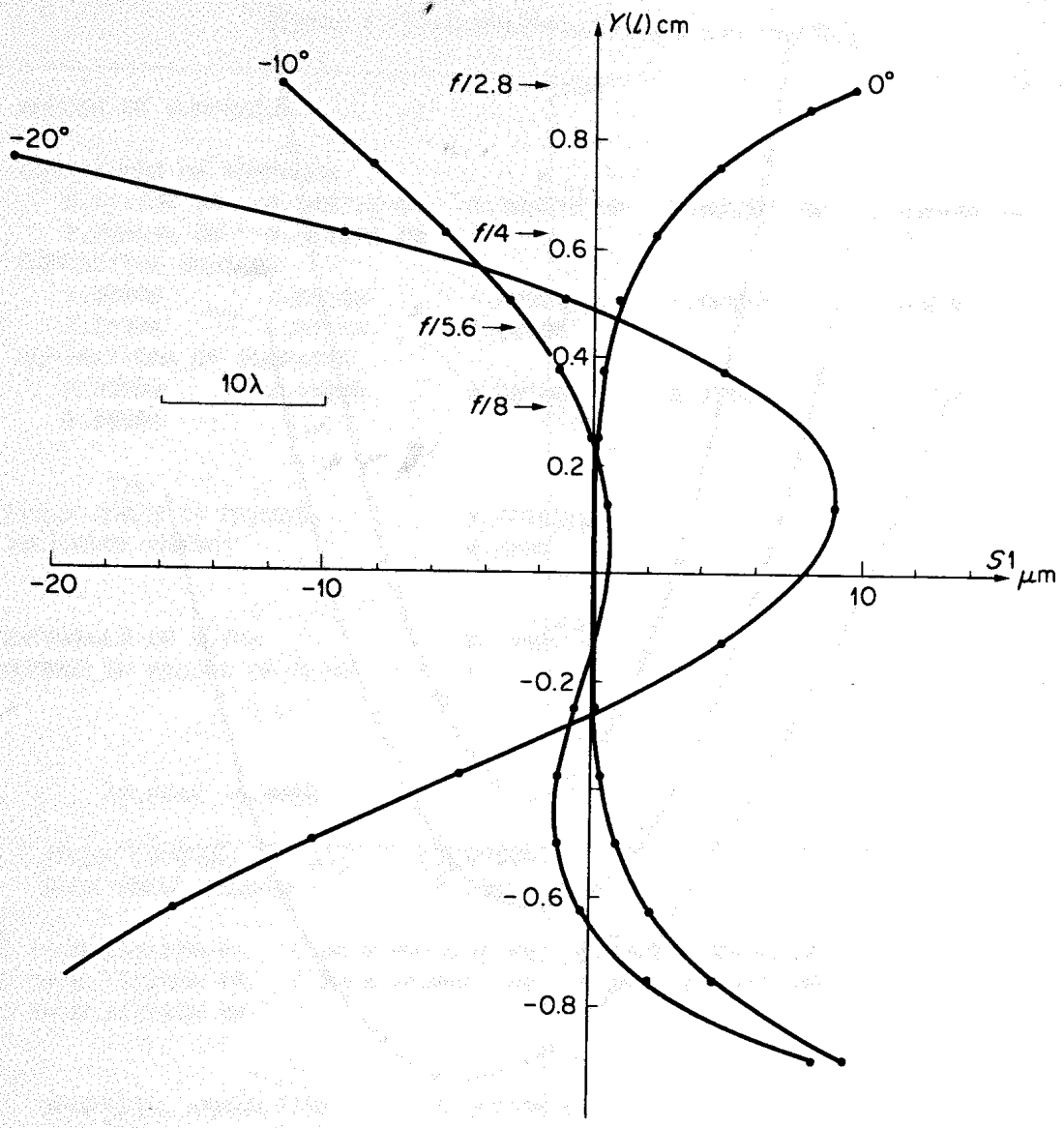

Figure 8a. Variation of $S1$ with aperture $Y(1)$ for various angles $U(1)$

in Table 3, and illustrated in Figure 8b. It is seen that the curves are roughly parabolic and this is usually the case. It is also seen that $S1$ can be exactly zero for some values of $U(1)$ and $Y(1)$, but that these do not occur at the same value of the bending parameter. From an examination of these curves and of those in Figure 8a it would appear that the TESSAR lens, as specified, is reasonably well corrected for spherical aberration but that it might be worth examining a lens as specified by $\Delta\alpha = -0.17$, $c(1) = 0.44758$ in order to see if the curves are flatter.

It is not wise to push the conclusions too far as we have considered only the effect of spherical aberration, whereas other aberrations, especially coma and astigmatism, become important as we move to larger angular fields and the minimization of these may be the more important criterion. Coma is

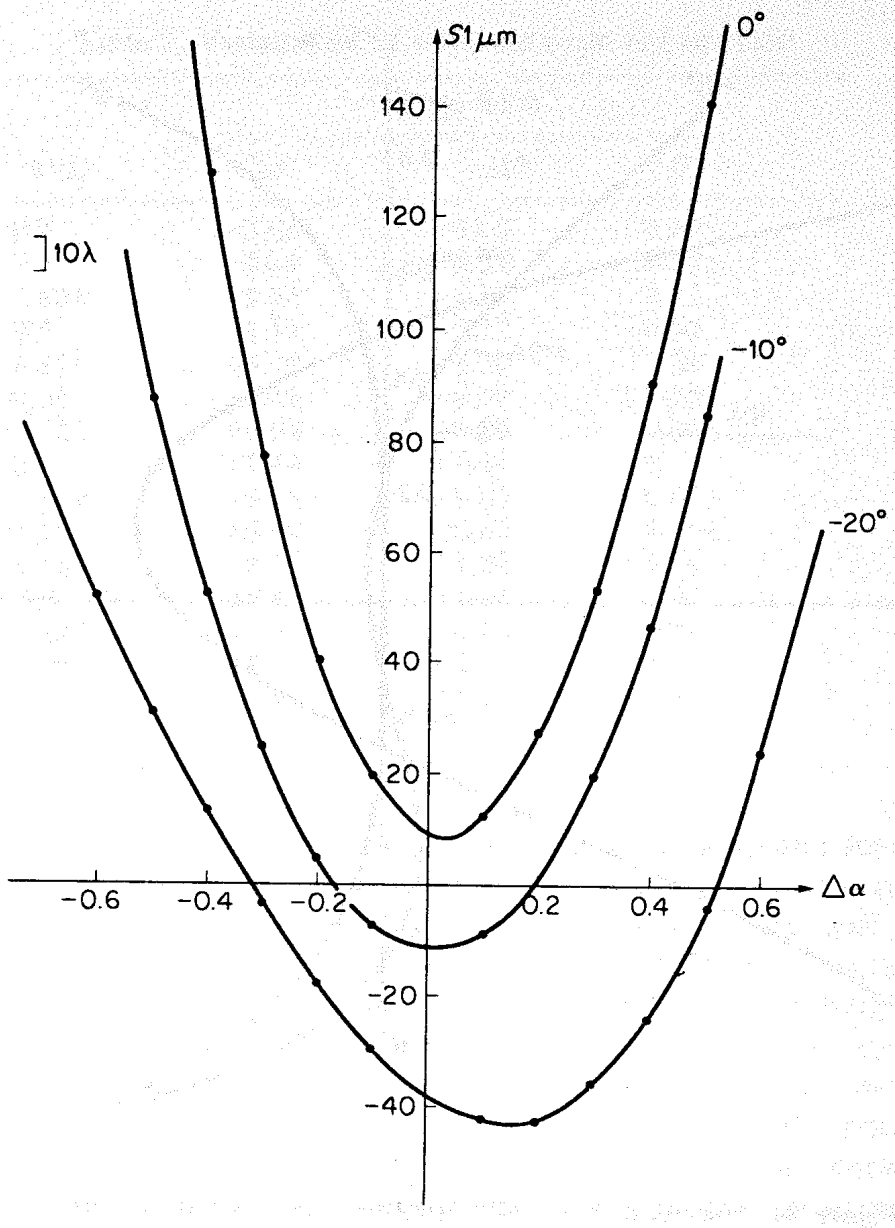

Figure 8b. Variation of $S1$ with bending parameter $\Delta\alpha$

usually a minimum near the turning point of the $S1$ parabola and indeed it can be shown that for the TESSAR it is near zero at $\Delta\alpha = 0$, ($U(1) = -20°$, $Y(1) = 0.9$).

8.3 Results from RAYTRC

Although the curves for $S1$ give a fair idea of the wavefront errors of the lens it is the pattern of light on the image plane that is of final interest, and the magnitude of the deviations from perfect imagery is realized by seeing

Table 3. Typical results from a lens bending

```
NUMBER OF SURFACES          7

CURVATURES OF SURFACES
   0.61425E 00  -0.36271E-01  -0.28927E 00   0.63221E 00   0.00000E 00
   0.52083E 00  -0.41667E 00
REFRACTIVE INDICES
   1.00000       1.61160       1.00000       1.60530       1.00000
   1.51230       1.61160       1.00000
SEPARATIONS OF SURFACES
   0.35700       0.18900       0.08100       0.32500       0.21700
   0.39600


FIELD ANGLE IN DEGREES          0.0000
INCIDENCE HEIGHT                0.9000


INTERVALS OF ALPHA              0.1000
NUMBER OF VALUES OF ALPHA      13


       DALPHA= -0.6000

   FOCAL LENGTH                5.07986
   BACK FOCAL LENGTH           5.72729

C 1=-0.524157E-01   C 2=-0.694984E 00   C 3=-0.976354E 00
C 4=-0.151389E 00   C 5=-0.692691E 00   C 6=-0.213361E 00
C 7=-0.911931E 00


   SPHERICAL ABERRATION        0.28279E-01


       DALPHA= -0.5000

   FOCAL LENGTH                5.07986
   BACK FOCAL LENGTH           5.50726

C 1= 0.586954E-01   C 2=-0.593528E 00   C 3=-0.871236E 00
C 4=-0.338594E-01   C 5=-0.588523E 00   C 6=-0.107366E 00
C 7=-0.845875E 00


   SPHERICAL ABERRATION        0.19605E-01
```

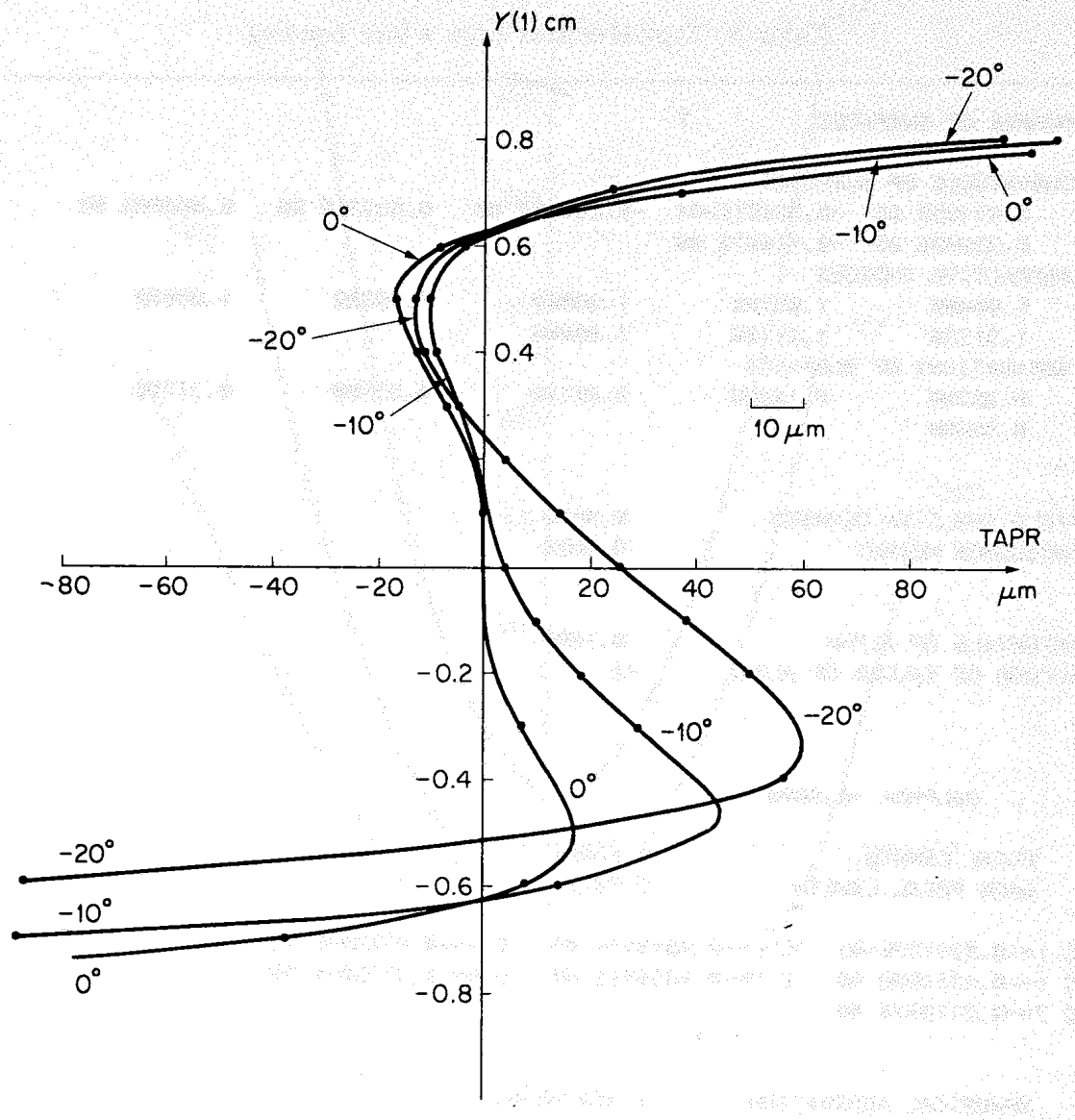

Figure 8c. Variation of the transverse aberration with aperture Y(1)

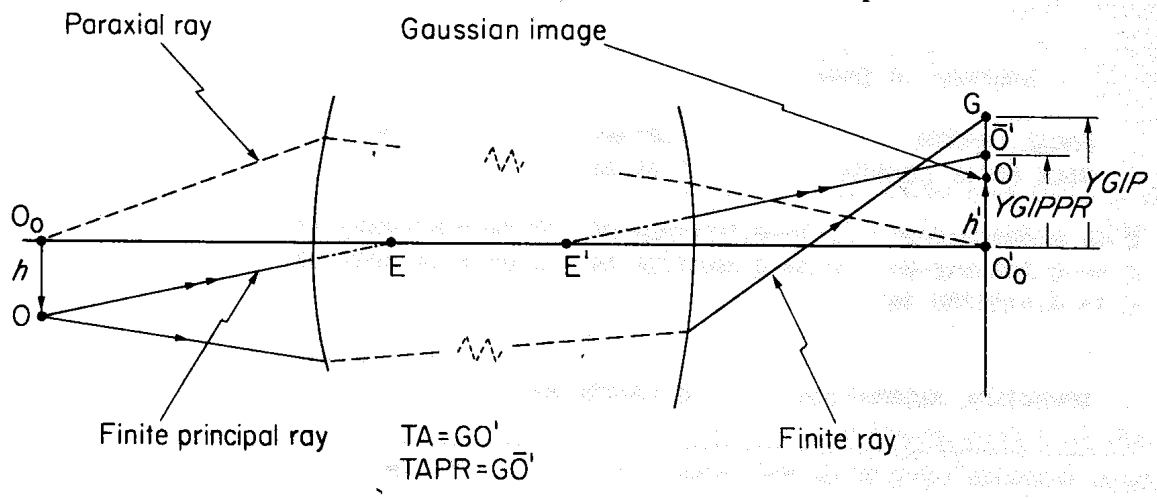

Figure 8d. Definition of transverse aberration quantities

how far the ray intersections on the image plane differ from each other and how far they deviate from the ideal image point upon which, for a perfect system, they should converge.

The program RAYTRC outputs, as a function of incident height $Y(1)$, the transverse aberrations TA and TAPR, where

$$\text{TA} = \text{YGIP} - \text{YPXL},$$

$$\text{TAPR} = \text{YGIP} - \text{YGIPPR},$$

YGIP is the ray intersection on the Gaussian image plane, TA is the transverse aberration with respect to the Gaussian image of height YPXL (YPXL $= h'$ of equation (15)), and TAPR is the transverse aberration with respect to the finite principal ray which intersects the Gaussian image plane at YGIPPR. If the finite principal ray does not intersect the image plane at the paraxial image point then the system suffers from distortion. The variables are illustrated in Figure 8d, in which O_0O is an object of height h, O'_0O' is the paraxial image of height h', $\bar{O}'$ is the finite principal ray intersection, and G is the finite ray intersection.

A typical output is shown at the end of the chapter and the results are plotted in Figure 8c. A comparison of the transverse aberrations with respect to the Gaussian image, TA, and with respect to the principal ray, TAPR, shows that they differ by about 630 μm giving a distortion of 0.63/17.5 or 3.5 per cent, which is just about acceptable at the edge of the field.

The spread about the principal ray image, i.e. the range of values of TAPR, is small between about $Y(1) = +0.65$ and $Y(1) = -0.5$ for the $-10°$ field, but only between $Y(1) = +0.65$ and $Y(1) = 0$ for the $-20°$ field. Actually as the eye, working at its least distance of distinct vision, can resolve distances of the order of 100 μm, then allowing for a magnification of 10×, ray deviations of 10 μm or less would be acceptable in the image. The system is therefore usable at f/4 provided a stop is introduced, probably near surface number 4 and made small enough to cut out the $-20°$ field rays entering the lower part of the lens. Note that no allowance is made in the program for the finite sizes of the lens elements other than the possibility that the rays miss the lens surface entirely. A more realistic trace would need the insertion of lens diameters.

9. SUGGESTIONS FOR FURTHER STUDY

The Tessar lens is a fairly complicated optical system that needs a great deal of analysis to realize its limitations and capabilities; however, it is instructive to carry out the investigation of some simpler systems using S1BEND and RAYTRC.

9.1 The single lens

It is shown, in most elementary optics texts,[10] that a single lens has minimum spherical aberration if:
(a) for an infinite object, it is nearly convexo-plane,
(b) for a finite object, it is biconvex.
These situations are illustrated in Figures 9a and 9b and the two results are readily checked by starting with a biconvex lens and bending it. Suitable starting values are given in Table 4.

It is also of interest to find how the $S1 \sim \Delta\alpha$ parabola shifts vertically as the refractive index is varied between 1.5 and 1.7, which corresponds to the range of readily available glasses.

9.2 The achromatic lens

One of the basic defects of all refracting systems is that, when they are used with white light, the refractive index varies with wavelength and hence the aberration also varies; however, the variation of $S1$ is of second order

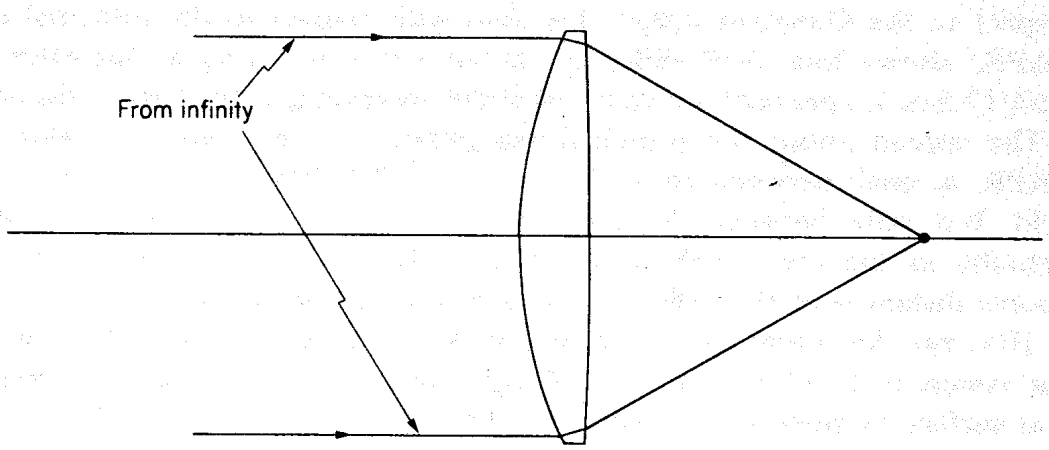

Figure 9a. Almost convexo-plane lens with minimum spherical aberration for object at infinity

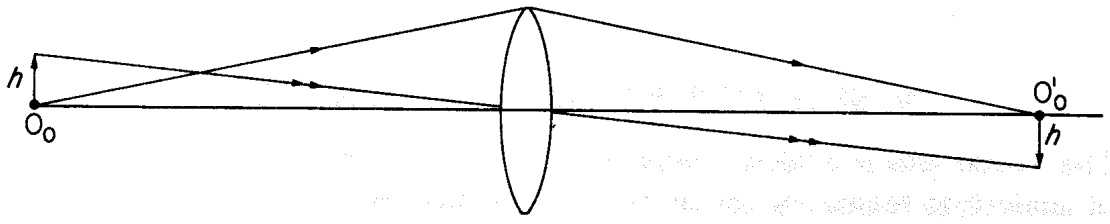

Figure 9b. Bi-convex lens with minimum spherical aberration for object imaged at unit magnification